NJC

Accepted Manuscript

ROYAL SOCIETY OF CHEMISTRY

www.rsc.org/njc

Rhodamine-Modified Upconversion Nanoprobe for Distinguish Cu^{2+} from Hg^{2+} and Living Cells Imaging

Yanxia Xu[a], Huifang Li[b], Xianfu Meng[a], Jinliang Liu*[a], Lining Sun[a], Xiaolin Fan[b] and Liyi Shi*[a]

[a] Research Center of Nano Science and Technology, Shanghai University, 200444, China.

[b] Key Laboratory of Organo-Pharmaceutical Chemistry, Gannan Normal University, Ganzhou 341000, P. R. China.

*To whom correspondence should be addressed:

Dr. Jinliang Liu

Research Center of Nano Science and Technology, Shanghai University, 200444, China.

Phone: +86-21-66137197

Fax: +86-21-66137197

Email: liujl@shu.edu.cn

Prof. Liyi Shi

Research Center of Nano Science and Technology, Shanghai University, 200444, China.

Phone: +86-21-66137208

Email: shiliyi@shu.edu.cn.

Abstract

It is greatly important to seek a fast and sensitive method for the detection of Cu^{2+} ion because of its vital role in human body. Fluorescent probes, especially the rhodamine derivatives, have been considered as promising candidates for detection of Cu^{2+} ion due to their attractive features. However, one problem frequently encountered in rhodamine-based fluorescent probes is that some of them could not distinguish Cu^{2+} from Hg^{2+} and these drawbacks limit their application in biological samples. In this paper, a rhodamine B derivative (RBH) was grafted to the mesoporous silica coated upconversion nanoparticles (CS-UCNP) to fabricate a new organic-inorganic hybrid nanoprobe. On the addition of Cu^{2+} ion, an emission band at about 580 nm appeared while the intensity of the green emission at about 545 nm of the nanoprobe decreased upon the excitation of a 980 nm laser, implying a luminescence resonance energy transfer (LRET) happened from the CS-UCNP to the RBH-Cu^{2+} complex. The obtained LRET nanoprobe could detect Cu^{2+} exclusively even at the present of Hg^{2+} with a detection limit of 0.82 μM in absolute ethanol solution. Most importantly, this nanoprobe can be used for monitoring subcellular distribution of Cu^{2+} in living cells based on upconversion luminescence and downconversion fluorescence.

Keywords: Upconversion nanoparticles; Detection; Cell imaging; Rhodamine B derivative

1. Introduction

Copper is one of the most important trace element and plays a vital role in the body of human beings, the dishomeostasis of coper ion could result in serious diseases, including Menkes and Wilson diseases,[1,2] Alzheimer's disease,[3] amyotrophic lateral sclerosis (ALS),[4] and even death. Accordingly, the development of probes for monitoring the trace level of Cu^{2+} ion in biological samples has drawn much attention during these years. The traditional method of detecting copper ion include atomic absorption spectrometry, inductively coupled plasma atomic emission spectrometry (ICP-AES), inductively coupled plasma mass spectroscopy (ICP-MS). These methods are always suffer from some drawbacks, such as low sensitivity, complicated pretreatment procedures, expensive instrumentation dependence, making them not suitable for on-line monitoring. Recently, fluorescent probes have been considered as promising candidates for detection of Cu^{2+} ion because of their sample, rapid and non-destructive characteristics. Some fluorescence sensors have been developed for detection of Cu^{2+} ion with high sensitivity and selectivity.[5-7] Among these report, rhodamine compounds have shown significant advantages over some traditional fluorophores due to their attractive feature such as high photostability, wide wavelength range and high fluorescence quantum yield, and thus become an extensive research topic in the field of chemical and biological.[8-14] However, one problem frequently encountered in rhodamine-based fluorescent probes is that, upon existence of Cu^{2+} and Hg^{2+} simultaneously, these probes could not distinguish them selectively. These drawbacks limit their application in biological samples.[15-17]

Compared to UV light, near-infrared (NIR) light has received increasing popularity as an excitation source due to its deeper tissue penetration and less damage for biological specimens.[18-21] Lanthanide-doped upconversion nanoparticles (UCNPs), which are capable of converting NIR

excitation light into shorter wavelength light have been proven to exhibit attractive optical and chemical properties, such as large stokes shifts, low toxicity, weak auto-fluorescence backgrounds, resistance to photo-bleaching[22-27]. In fact, these merits make UCNPs an ideal candidate as the luminescence donor in luminescence resonance energy transfer (LRET) nanoprobe. For example, Chu et al. assembled phospholipid-modified upconversion nanoparticle with rhodamine B via the hydrophobic van der Waals interactions for the detection of phospholipase D.[28] Wang et al. presented a novel dual LRET system for the detection of Hg^{2+} and Pb^{2+} simultaneously by using gold nanoparticles (AuNPs) as efficient energy acceptors and two kinds of upconversion nanoparticles as efficient energy donors.[29] Li et al. constructed a biosensing platform by combining the ssDNA-modified UCNPs and graphene oxide (GO) materials acceptors via a strong π-π stacking effect between nucleobases of ssDNA and sp^2 atoms of GO.[30]

Recently, Li and co-authors' reported a rhodamine B derivative 4 containing a highly electron-rich S atom to serve as a fluorescence turn-on chemodosimeter for Cu^{2+}. However, this chemodosimeter could not distinguish Cu^{2+} from Hg^{2+} because both of them can arouse the similar "turn-on" fluorescence and the color change from colorless to purple[7]. Considering that the S atom in rhodamine B derivative 4 plays a key role in the response towards Hg^{2+}, in this work, by substituting S atom with O atom, a rhodamine B derivative was presented and then grafted to the mesoporous silica ($mSiO_2$) coated upconversion nanoparticles to fabricate an organic-inorganic hybrid nanoprobe, in which the core-shell structured upconversion nanoparticles $NaYF_4$:Yb,Er@$NaYF_4$ (CS-UCNP) and rhodamine B derivative served as energy donor and energy acceptor, respectively. Benefited from the one-atom exchange (from S atom to O atom), the obtained nanoprobe could detect Cu^{2+} exclusively even at the present of Hg^{2+}, which was often thought of as the most interferential ion to Cu^{2+}. Most importantly, this nanoprobe can be used for

monitoring subcellular distribution of Cu^{2+} in living cells based on upconversion luminescence (UCL) and downconversion fluorescence.

2. Experimental

2.1 Materials

All the chemicals were used without further purification: $YCl_3 \cdot 6H_2O$ (99.99%), $YbCl_3 \cdot 6H_2O$ (99.99%), $ErCl_3 \cdot 6H_2O$ (99.99%), tetraethyl orthosilicate (TEOS, >99%) were purchased from Sigma Aldrich. Oleic acid (90%, technical grade) was purchased from Alfa Aesar. Octadecene (90%, technical grade), methanol (99.5%), 3-(triethoxysilyl)propyl isothiocyanate (95%, Guaranteed reagent), ammonium fluoride (NH_4F, ACS, 98%), sodium hydroxide (NaOH, reagent grade, $\geq$98%), and cetyltrimethylammonium bromide (CTAB, >99%) were purchased from Aladin Company. Rhodamine B (RhB, 95%), hydrazine hydrate 80 wt.% solution in H_2O were purchased from J & K Technology Co., Ltd. Acetone (99.5%, analytial reagent), cyclohexane (99.5%, analytial reagent), anhydrous ethanol (99.7%, analytial reagent), toluene (99.5%, analytial reagent), ammonium nitrate (NH_4NO_3, $\geq$99.0%), and hydrochloric acid (HCl, 36%-38%, analytial reagent) were obtained from Sinopharm Chemical Reagent Co., Ltd. Deionized water was used to prepare all aqueous solutions. Solutions of Cu^{2+}, Hg^{2+}, Mn^{2+}, Na^+, K^+, Fe^{3+}, Cr^{3+}, Mg^{2+}, Ni^{2+}, K^+ and Ca^{2+} were prepared from their chloride salts, solutions of Zn^{2+}, Co^{2+}, Fe^{2+}, and Li^+ were prepared from zinc acetate dihydrate, cobaltous nitrate, ferrous sulfate, and lithium fluoride, respectively.

2.2 Synthesis of NaYF$_4$:Yb,Er (UCNP) and NaYF$_4$:Yb,Er@NaYF$_4$ (CS-UCNP)

The β-phase $NaYF_4$:Yb,Er nanocrystals was synthesized via a solvothermal method.[31] 1.56 mL of YCl_3 (1.0 M), 0.40 mL of $YbCl_3$ (1.0 M) and 0.40 mL of $ErCl_3$ (0.10 M) were added to a 100 mL two-necked flask and the mixture was heated to 110 ^{o}C to evaporate the water, then, 12 mL of oleic acid and 30 mL of 1-octadecene were added and the mixture were heated to 150 ^{o}C. After cooling to

room temperature, 20 mL of methanol solution containing NH_4F (0.3 g, 8 mmol) and NaOH (0.2 g, 5 mmol) was added and the solution was stirred at 110 °C to remove methanol and residual water. The resultant solution was then heated to 300 °C under N_2 atmosphere for 1h. The obtained suspension was separated by centrifugation and washed with cyclohexane and acetone for three times and then dispersed in 20 mL of cyclohexane. The synthesis procedure of $NaYF_4$:Yb,Er@$NaYF_4$ nanoparticles was similar to that of $NaYF_4$:Yb,Er except that 0.80 mL of $YbCl_3$ (1.0 M) was replaced by 5.0 mL of the prepared $NaYF_4$:Yb,Er.

2.3 Synthesis of CS-UCNP@$mSiO_2$ nanoparticles

0.1 g of CTAB was dissolved in 20 mL of deionized water, and then 2 mL of cyclohexane solution containing the core-shell nanoparticles (4 mg mL^{-1}) was added. The mixture was stirred vigorously to evaporate the cyclohexane solvent. For silica coating, 10 mL of the aqueous CTAB stabilized nanoparticles solution was added to a mixture of 20 mL of deionized water, 3.0 mL of ethanol and 150 μL of 2.0 M NaOH. The mixture was heated to 70 °C under stirring. 200 μL of TEOS was then added dropwise and the heating was maintained for another 2 h with vigorous stirring. After cooling to room temperature, the nanoparticles were centrifuged and washed with anhydrous ethanol 4 times. The surfactants were removed via a fast and efficient ion exchange method,[32] and then dispersed in 10 mL of ethanol for further use.

2.4 Synthesis of Rhodamine B hydrazide (RBH)

RBH were prepared as previously reported.[5] 5 g (10 mmol) of rhodamine B was dissolved in anhydrous ethanol and 12 mL (200 mmol) of hydrazine hydrate was added dropwise. The mixture was heated to 100 °C and maintained for 8 h with vigorous stirring under N_2 atmosphere. After cooling to room temperature, the solvent was removed under reduced pressure. The precipitate was washed by deionized water and dried under reduced pressure. ^{1}H NMR (CDCl$_3$): δ (ppm) : 7.92 (d,

1H, ArH), 7.44 (t, 2H, ArH)，7.09 (d, 1H, ArH), 6.46 (s, 2H, xanthene-H), 6.41 (d, 2H, xanthene-H),

6.29 (d, 2H, xanthene-H), 3.6 (s, 2H, NH_2), 3.33 (q, 8H, NCH_2CH_3), 1.16 (t, 12H, NCH_2CH_3).

2.5 Synthesis of CS-UCNP@mSiO$_2$-RBH nanoparticles

40 mg of CS-UCNP@mSiO$_2$ nanoparticles were dissolved in 20 mL of toluene and 20 μL of

3-(triethoxysilyl) propyl isothiocyanate was added. The mixture was stirred under argon for 24 h.

After cooling to room temperature, RBH (80 mg) was added and the mixture was refluxed for

another 24 h. The nanoparticles were separated by centrifugation at 8000 rpm for10 min, washed

several times with anhydrous ethanol. The obtained nanoparticles were dispersed in 10 mL of

anhydrous ethanol for further use.

2.6 Detection of Cu^{2+} ion

Stock solutions of Cu^{2+} (0.02 M), other metal ions (0.1 M) were prepared in deionized water.

The solution of CS-UCNP@mSiO$_2$-RBH nanoparticles (3 mg/mL) was prepared in absolute ethanol

solution. For titration experiments, the Cu^{2+} stock solution was added to 2.0 mL of

CS-UCNP@mSiO$_2$-RBH solution by using a micropipette, and then UV-Vis absorption and

fluorescence spectra were recorded. For selectivity experiments, the test samples were prepared by

adding appropriate amounts of metal ions solution to 2.0 mL of the hybrid nano-probe

CS-UCNP@mSiO$_2$-RBH. For competition experiments, Cu^{2+} was added to the solutions containing

CS-UCNP@mSiO$_2$-RBH and other metal ions of interest. All solutions were stirred for 1 min

before the spectral test. For downconversion fluorescence measurements, excitation was fixed at

520 nm, and emission was collected from 535 to 700 nm, and for upconversion luminescence

measurements, excitation was fixed at 980 nm, and emission was collected from 450 to 680 nm.

2.7 Cell culture

Human cervical carcinoma HeLa cells were provided by the Institute of Biochemistry and Cell

Biology, SIBS, CAS (China). The cells were grown in RPMI 1640 supplemented with 10% FBS at

37 $^{\circ}$C and 5% CO_2. Cells (1×10^5 cells mL^{-1}) were plated on 14 mm glass coverslips and allowed to

adhere for 24 h.

2.8 Cell imaging

Before the experiments, HeLa cells were washed with PBS buffer, and then incubated with 0.2

mg mL^{-1} CS-UCNP@mSiO$_2$-RBH in PBS for 2 h at 37 $^{\circ}$C, after that, the cells were incubated with

10 μM of Cu^{2+} for 0.5 h at 37 $^{\circ}$C. Cell imaging was then carried out after washing with PBS.

Confocal fluorescence imaging was performed with an OLYMPUS IX81 laser scanning microscope

and a 60P oil-immersion objective lens. Cells loaded with CS-UCNP@mSiO$_2$-RBH were excited at

543 nm using a HeNe laser. Emission was collected from 560 nm to 600 nm. Upconversion

luminescence imaging of Hela cells were executed on laser scanning upconversion luminescence

microscope (LSUCLM) under the excitation of CW 980 nm laser. Emission was collected from 520

nm to 560 nm.

2.9 Cytotoxicity assay

The methyl thiazolyl tetrazolium (MTT) assays were used to probe cellular viability. Hela cells

were cultivated in a 96-well cell-culture plate at a density of 10^4 per well under 100 % humidity for

12 h at 37 °C and 5% CO_2. After that, the medium was substituted for fresh medium at different

concentrations of CS-UCNP@mSiO$_2$-RBH (0, 100, 200, 300, 400, 500 μg mL^{-1}). After 24 h, the

medium containing nanoparticles were removed and 10 mL, 3 mg mL^{-1} of MTT solutions

(dissolved in RPMI 1640) were added and the plate was incubated for an additional 4 h at the same

condition. The cellular viability was calculated by the following formula: Viability (%) = total

viable cells/total cells (viable and non-viable) $\times 100$.[33]

2.10 Characterization

Sizes and morphologies of nanoparticles were determined at a JEM-200CX transmission electron microscope operated at 120 kV and 200 kV using a JEM-2010F high-resolution transmission electron microscope (HR-TEM). Samples of the as-prepared nanoparticles were prepared by placing a drop of dilute aqueous dispersions on the surface of a copper grid. X-ray diffraction (XRD) measurements were carried out on a D\max-2200 X-ray diffractometer using Cu Kα (λ = 1.54 Å) radiation. Fourier transform infrared spectroscopy (FT-IR) spectra were acquired in the spectral range from 4000 to 400 cm^{-1} with an Avatar 370 by using pressed KBr pellet technique. UV-Vis absorption spectra were recorded on a 760CRT dual beam spectrophotometer. Fluorescence spectra were determined on a LS-55 fluorescence spectrometer. The upconversion luminescent excitation and emission spectra were obtained on an Edinburgh FLS 920 luminescence spectrometer equipped with an external 0-800 mW 980 nm adjustable CW laser. ^1H NMR spectra were performed on an AVANCE 500 MHz spectrometer. The measurements mentioned above were conducted at room temperature (about 298K). Nitrogen (N_2) adsorption/desorption isotherms were measured by using a Nova l000 analyzer with nitrogen. The samples were outgassed for 4 h at 120 °C before the measurements. Surface areas were calculated by the Brunauer-Emmett-Teller (BET) method and pore sizes by the Barrett-Joyner-Halenda (BJH) methods. Thermogravimetric analysis (TGA) was performed on a Perkin-Elmer Pyris Diamond thermal analyzer up to 800 ^oC at a heating rate of 10 ^oC min $^{-1}$ under N_2.

2.11 Computational Details

Copper complexes were optimized with density functional theory (DFT)[34] using the Becke's three-parameter hybrid exchange functional combined with the Lee-Yang-Parr correlation functional (B3LYP)[35,36]. The "double-ζ" quality basis set LANL2DZ and corresponding effective core potentials[37-39] were used for Cu(II), while the 6-31G(p,d)[40] basis set was used for all other

atoms. All optimized configurations were confirmed to be minima on the potential energy surfaces by performing vibrational frequency calculations at the same level. In addition, a conductor-like polarizable continuum model (CPCM)[41] using ethanol (ε = 24.852) as the solvent was considered for optimization calculations of the involved geometries. Calculations were performed with Gaussian 09 (Revision D.01)[42].

3. Results and discussion

3.1 Characterization of the nanoprobe CS-UCNP@mSiO$_2$-RBH

The synthetic procedure for organic-inorganic hybrid nanoprobe (CS-UCNP@mSiO$_2$-RBH) is presented in Scheme 1. The UCNP nanocrystals were hydrophobic and can be well-dispersed in cyclohexane. As shown in Fig. 1a, the nanocrystals were uniform with an average diameter of 28-30 nm. After coated with a NaYF$_4$ layer, the obtained CS-UCNP were still fairly uniform and highly mono-disperse, and the particles size reached to 33-35 nm in diameter (Fig. 1b). Compared with the corresponding single type nanoparticles, the luminescence of core-shell nanoparticles was significantly enhanced. As shown in Fig. S1 (See Supporting Information), both the UCNP and CS-UCNP exhibited the similar emission peaks at 521, 542, and 654 nm when excited by 980 nm laser, which were attributed to the $^2H_{11/2} \rightarrow {}^4I_{15/2}$, $^4S_{3/2} \rightarrow {}^4I_{15/2}$, and $^4F_{9/2} \rightarrow {}^4I_{15/2}$ transitions of Er^{3+} ion, respectively.[43] The luminescence intensity of CS-UCNP is about 8 times larger than that of UCNP, demonstrated that the core-shell structure nanoparticle can be serve as an ideal energy donor to fabricate LRET-based nanoprobe.
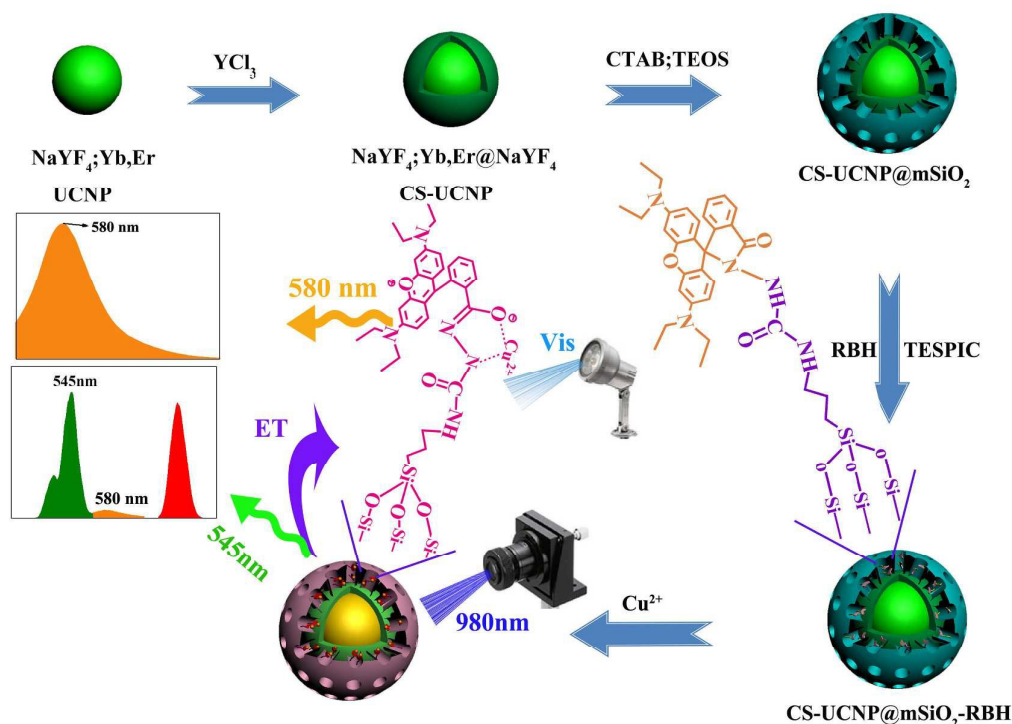
Scheme 1. Schematic illustration of the synthetic procedure of the CS-UCNP@mSiO$_2$-RBH and the proposed sensing mechanism of CS-UCNP@mSiO$_2$-RBH with Cu^{2+} ion.

Then, a mesoporous SiO$_2$ layer was coated on CS-UCNP and furtherly grafted with RBH to construct the nanoprobe. As shown in Fig. 1c, the mesoporous silica coated nanoparticles CS-UCNP@mSiO$_2$ were mono-dispersed and uniform in ethanol with an average diameter of 85-100 nm. Following immobilization of the RBH, the diameter of the CS-UCNP@mSiO$_2$-RBH was not significantly changed, and no aggregates were observed (Fig. 1d).
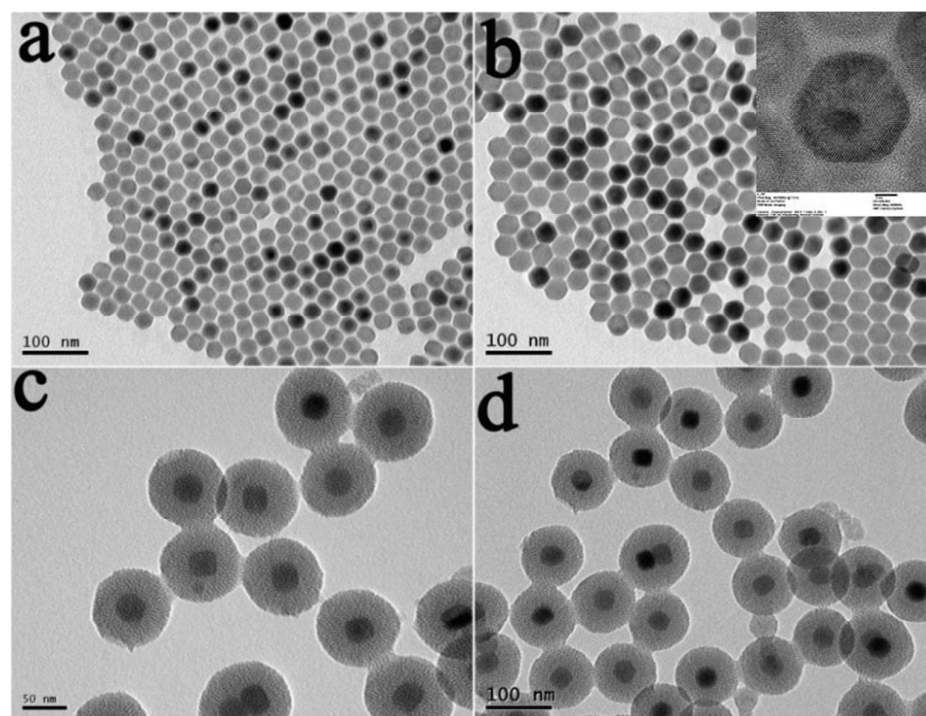
Fig. 1.TEM images of UCNP (a), CS-UCNP (b) dispersed in cyclohexane, CS-UCNP@mSiO$_2$ (c),

CS-UCNP@mSiO$_2$-RBH (d) dispersed in ethanol. Inset: HR-TEM images of CS-UCNP.

The XRD patterns of CS-UCNP@mSiO$_2$ and CS-UCNP@mSiO$_2$-RBH were shown in Fig.

S2A (See Supporting Information). Both of them show the similar diffraction peaks at the range of

10°-90°. The broad peak centered around 23° in the XRD patterns may be ascribed to the coherent

diffusion of the siliceous layer of these nanoparticles, while the main diffraction peaks are ascribed

to the pure hexagonal NaYF$_4$ structure (JCPDS No.16-0334). Small-angle X-ray diffraction

(SAXRD) patterns of CS-UCNP@mSiO$_2$ and CS-UCNP@mSiO$_2$-RBH samples were shown in Fig.

S2B (See Supporting Information). For CS-UCNP@mSiO$_2$, two characteristic diffraction peaks (2θ

= 2.0^o, 4.2^o) were observed, which can be indexed to (100) and (110) diffractions and assigned to

the two-dimensional hexagonal (P6mm) symmetry. For CS-UCNP@mSiO$_2$-RBH, the intensity of

the XRD pattern is decreased slightly, indicating a less ordered mesostructured achieved. This is

attributable to the attachment of the RBH to the mesoporous pores of the silica shell.

The mesoporous silica layer modification of CS-UCNP and the grafting with RBH were also

confirmed by FT-IR spectroscopy. As shown in Fig. S3 (See Supporting Information), the peaks at

1080 cm^{-1} and 550 cm^{-1} in the FT-IR spectrum of CS-UCNP@mSiO$_2$ and CS-UCNP@mSiO$_2$-RBH

can be ascribed to the stretching vibrations of the Si-O-Si and Si-O group of silica, demonstrating

the successful silica coating modification of CS-UCNP. For CS-UCNP@mSiO$_2$-RBH, the new

transmission bands at 2982 cm^{-1} and 2920 cm^{-1} were assigned to the asymmetric and symmetric

stretching vibrations of methylene (CH$_2$), respectively, and the bands at 1630, 1590 and 1392 cm^{-1}

were attributed to the stretching vibration of the =C-H bond in the phenyl group of the attached

rhodamine, suggesting the successful grafting of RBH in the CS-UCNP@mSiO$_2$ samples. The

nitrogen adsorption-desorption isotherms and pore-size distribution data of the nanoparticles were

shown in Fig. 2A. The BET analysis results show that BET surface area and pore volume of

CS-UCNP@mSiO$_2$ were 1039 m^{2}g^{-1} and 0.95 cm^{2}g^{-1}, respectively. A narrow pore size distribution

of 2.78 nm was obtained using the BJH method. When RBH molecules were grafted into the

mesoporous pores of the silica shell, the surface area and pore size have decreased to 973 m^{2}g^{-1} and

2.53 nm, respectively. The decrease in surface area and pore diameter in CS-UCNP@mSiO$_2$-RBH

is attributed to the attachment of the RBH to the inner channels of the silica. Furthermore, The RBH

concentration of CS-UCNP@mSiO$_2$-RBH was calculated to be 5.3 wt% as determined by TGA of

CS-UCNP@mSiO$_2$ and CS-UCNP@mSiO$_2$-RBH. (Fig. S4, See Supporting Information)
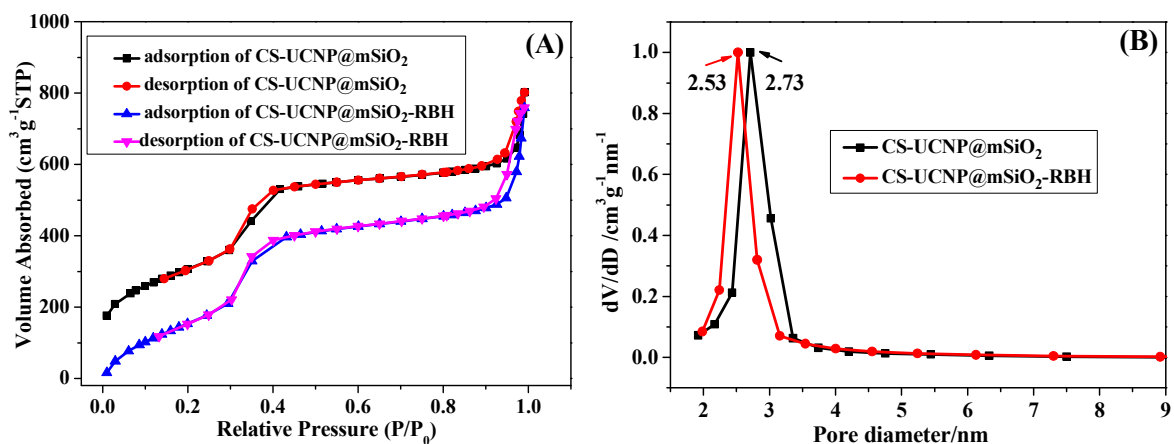
Fig. 2. The nitrogen adsorption-desorption isotherms (A) and pore-size distribution data (B) of CS-UCNP@mSiO$_2$ and CS-UCNP@mSiO$_2$-RBH.

3.2 Detection of copper ion in vitro

The UV-Vis absorption spectra of CS-UCNP@mSiO$_2$-RBH towards various metal ions were illustrated in Fig. 3A. The spectra of CS-UCNP@mSiO$_2$-RBH in absolute ethanol exhibited only a weak band above 500 nm, indicating the mainly existence of closed spirolactam ring of the rhodamine fluorophore. Upon the addition of Cu^{2+}, the absorbance was significantly enhanced and a new peak at 555 nm was observed in the absorption spectrum, which was ascribed to the formation of delocalized xanthane moiety of rhodamine and the ring opening of spirolactam. The proposed sensing mechanism of CS-UCNP@mSiO$_2$-RBH with Cu^{2+} ion was shown in Scheme 1. Upon addition of Cu^{2+}, a 1:1 stoichiometry complex between CS-UCNP@mSiO$_2$-RBH and Cu^{2+} formed, which gave rise to ring-opening reaction of the rhodamine group from the nanoprobe. The proposed mechanism was in consistent with our computational results, in which copper complexes were optimized with density functional theory (DFT) using the Becke's three-parameter hybrid exchange functional combined with the Lee-Yang-Parr correlation functional (B3LYP). (Fig. S5, See Supporting Information) Other metal ions, including Fe^{2+}, Fe^{3+}, Ca^{2+}, Mg^{2+}, Ni^{2+}, Na^{+}, Ba^{2+}, Cr^{3+}, K^{+}, Mn^{2+}, Zn^{2+}, Co^{2+}, and Li^{+}, had little interference, even Hg^{2+} which was often thought of as the most interferential ion to Cu^{2+}, indicating that this nanoprobe can detect Cu^{2+} exclusively. Fig. 3B shows the UV-Vis titration spectra of CS-UCNP@mSiO$_2$-RBH solution (3 mg/mL) upon the addition of different concentrations of Cu^{2+} ion. Upon the addition of Cu^{2+} gradually, the intensity of the absorption band centered at 555 nm increases evidently, indicating the undergoing of the ring-open process of the rhodamine B unit in CS-UCNP@mSiO$_2$-RBH. A linear increase of the absorbance intensity can be observed with the increasing of Cu^{2+} in a wide range from 0 to 400 μM

(See inset of Fig. 3B) with a 15-fold increase of absorbance. According to the formula, the detection

limit LOD = $3S_0/S$ (where 3 is the factor at the 99% confidence level, S_0 the standard deviation of

the blank measurements, and S is the slope of the calibration curve), the LOD of this nanoprobe

towards Cu^{2+} was calculated to be 2.56 µM (Fig. S6A, See Supporting Information). Furthermore,

the color change of CS-UCNP@mSiO$_2$-RBH solution upon the addition of various metal ions was

shown in Fig. 3C. Only an obvious purple color could be observed in the presence of Cu^{2+},

suggested that the nanoprobe CS-UCNP@mSiO$_2$-RBH could serve as "naked-eye" chemosensor for
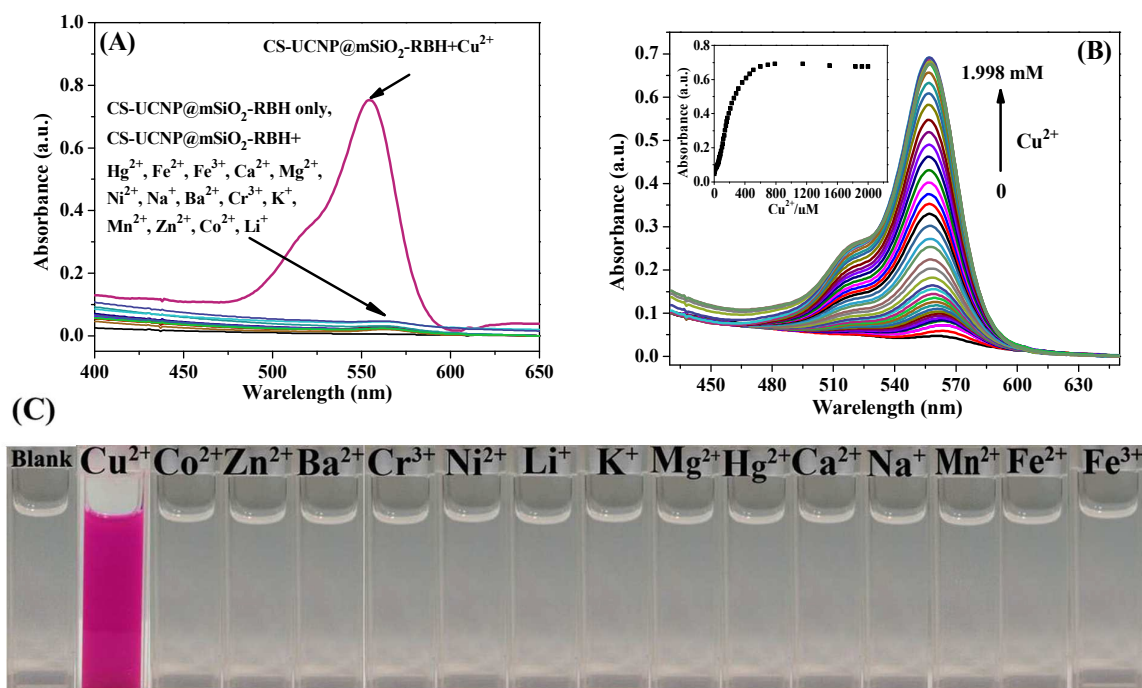
Cu^{2+}.

Fig. 3. (A) UV-vis absorption spectra of CS-UCNP@mSiO$_2$-RBH upon the addition of 20 µL of

various metal ions (Hg^{2+}, Ca^{2+}, Mg^{2+}, Ni^{2+}, Na^+, Ba^{2+}, Cr^{3+}, K^+, Mn^{2+}, Zn^{2+}, Co^{2+}, Li^+, Cu^{2+}, Fe^{2+},

Fe^{3+}) in absolute ethanol. (B) Absorption changes of CS-UCNP@mSiO$_2$-RBH with increasing

amounts of Cu^{2+} ion. Inset: absorbance at 555 nm as a function of Cu^{2+} concentration. (C) The

colorimetric performance of the solution upon the addition of various metal ions.

The fluorescence spectra of CS-UCNP@mSiO$_2$-RBH towards various metal ions were

illustrated in Fig. 4A. Only the addition of Cu^{2+} could induce a significant enhancement of fluorescence intensity at 580 nm, which was consistent with the results from the UV-Vis absorption spectra. Correspondingly, significant enhancements in fluorescence intensity at 580 nm (above 10 fold) can be observed in the fluorescence titration spectra of CS-UCNP@mSiO$_2$-RBH solution (3 mg/mL) upon the addition of different concentrations Cu^{2+} ion (Fig. 4B), and an orange color was obtained from the fluorescence image of CS-UCNP@mSiO$_2$-RBH solution in the presence of Cu^{2+} ion (Fig. 4C). The detection limit for Cu^{2+} was calculated to be 0.82 μM, suggesting that the nanoprobe could sensitively detect environmentally relevant levels of Cu^{2+} by using fluorescence technic. (Fig. S6B, See Supporting Information) Moreover, the competition experiment revealed that the Cu^{2+}-induced absorbance intensity was not influenced by the subsequent addition of competitive cations (Fig. S7, the red bars, See the Supporting Information). Obviously, these results confirmed that the nanoprobe owned remarkably high sensitivity and selectivity toward Cu^{2+} ion over other competitive cations.
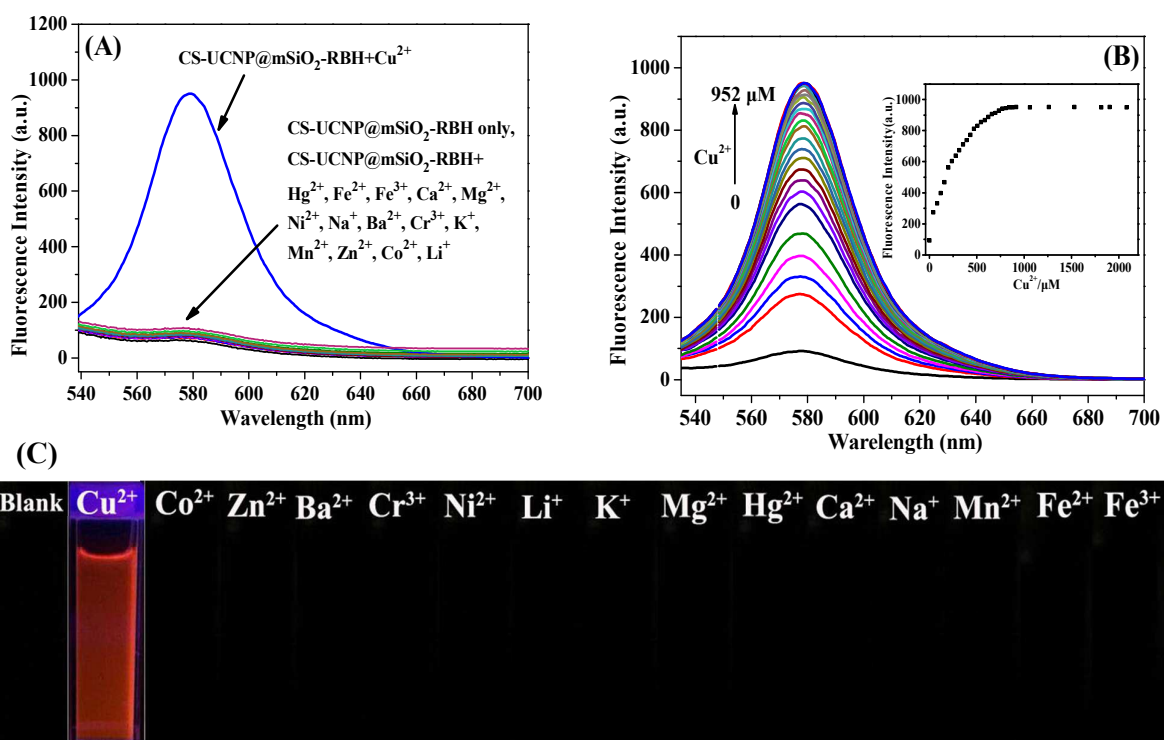
Fig. 4. (A) Fluorescence spectra of CS-UCNP@mSiO$_2$-RBH upon the addition of 20 μL of various metal ions (Hg^{2+}, Ca^{2+}, Mg^{2+}, Ni^{2+}, Na$^+$, Ba^{2+}, Cr^{3+}, K$^+$, Mn^{2+}, Zn^{2+}, Co^{2+}, Li$^+$, Cu^{2+}, Fe^{2+}, Fe^{3+}) in absolute ethanol solution. (B) Fluorescence responses of CS-UCNP@mSiO$_2$-RBH with increasing amounts of Cu^{2+} ion. Excitation was performed at 520 nm. Inset: fluorescence at 580 nm as a function of Cu^{2+} ion concentration. (C) The fluorescence changes of the solution upon addition of various metal ions.

Under the excitation of CW 980 nm laser, the synthesized CS-UCNP exhibited a strong green UCL emission with the peaks at 534~561 nm, which well matched the main absorption of RBH-Cu^{2+} complex (Fig. 5A). Based on the high spectral overlap between them, in CS-UCNP@mSiO$_2$-RBH nanoprobe, CS-UCNP was certainly arranged as energy donors that transferred its green light energy to the attached RBH-Cu^{2+} complex (Scheme 1 A). The UCL emission spectra of CS-UCNP@mSiO$_2$-RBH under different concentrations of Cu^{2+} ion were presented in Fig. 5B. It can be seen that the intensity of green emission at 526 nm and 545 nm of CS-UCNP@mSiO$_2$-RBH decreases gradually with the increasing of Cu^{2+} ion concentration, a broad emission band at about 580 nm appears, corresponding to the emission of the RBH-Cu^{2+} complex. Correspondingly, the photos of CS-UCNP@mSiO$_2$-RBH solution exhibited the green luminescence, and after the addition of Cu^{2+}, the color of the mixed solution changed to orange under 980 nm irradiation. (Inset in Fig. 5B) The decreasing of the green emission and the emergence of the broad band at about 580 nm demonstrated the energy transfer from the CS-UCNP to the RBH-Cu^{2+} complex. As the ratio of the emission intensity at 580 nm ($I_{580\ nm}$) to the intensity of 545 nm ($I_{545\ nm}$) is dependent on the concentration of Cu^{2+}, it is possible to use the CS-UCNP@mSiO$_2$-RBH as the nano ratio probe for detection of Cu^{2+} ion.
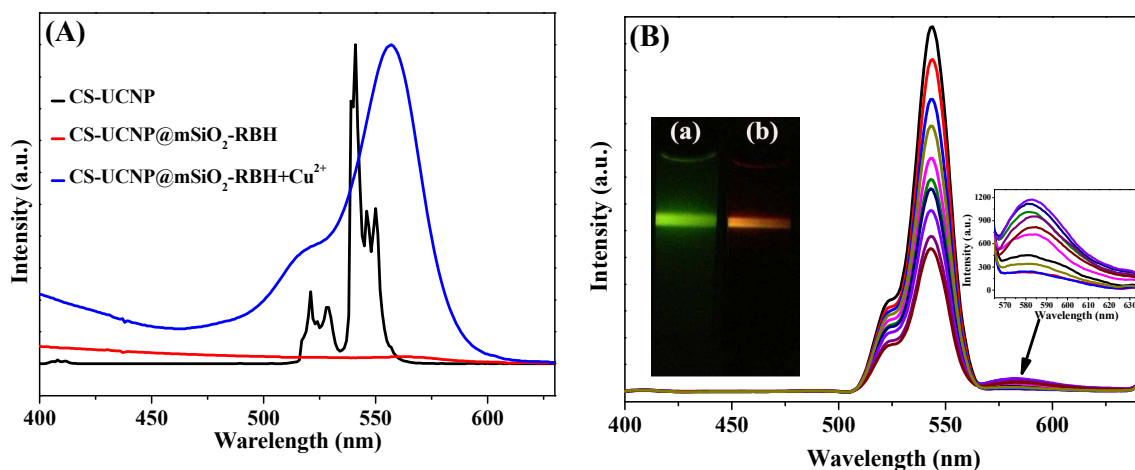
Fig. 5. (A) The upconversion emission spectrum of the CS-UCNP and the absorption spectra of CS-UCNP@mSiO$_2$-RBH and CS-UCNP@mSiO$_2$-RBH upon addition of Cu^{2+}. (B) Upconversion emission spectra of CS-UCNP@mSiO$_2$-RBH upon addition of 0-690 μM of Cu^{2+} ion in absolute ethanol solution upon 980 nm excitation. Inset: the photos of CS-UCNP@mSiO$_2$-RBH solution before (a) and after (b) the addition of Cu^{2+} ion under 980 nm irradiation.

The time dependence of the response of CS-UCNP@mSiO$_2$-RBH towrds Cu^{2+} was monitored by means of fluorescence spectroscopy. As shown in Fig. 6A, the response of CS-UCNP@mSiO$_2$-RBH (3 mg/mL) towards Cu^{2+} (950 μM) was rapid and a maximal signal was obtained within 1 min. The results demonstrated that the nanoprobe could be used to monitor Cu^{2+} in real time. Furthermore, the pH dependence of the Cu^{2+} sensing by CS-UCNP@mSiO$_2$-RBH was also studied. As shown in Fig. 6B, the fluorescence of the free nanoprobe CS-UCNP@mSiO$_2$-RBH can be negligible under a pH range from 4.1 to 10. After the addition of Cu^{2+}, the fluorescence of nano probe at 580 nm rapidly increased to a maximum value. The results showed that the nanoprobe can be worked within a wide pH range of 4.1-10.
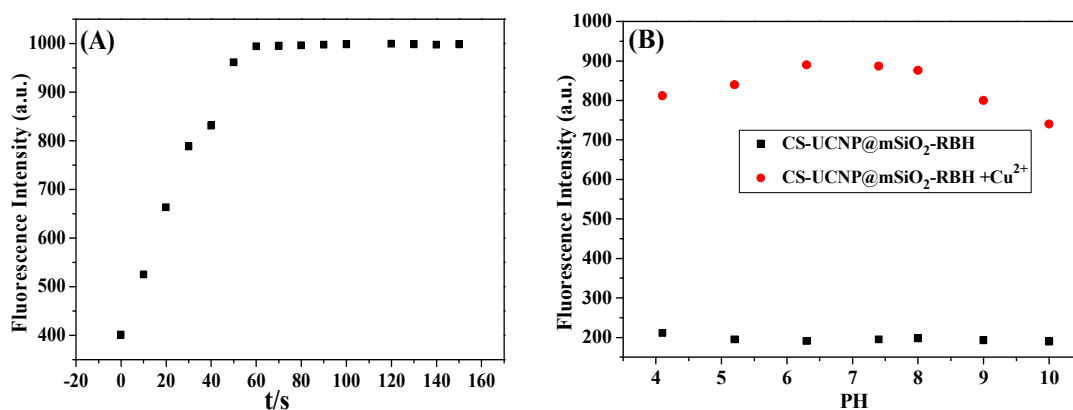
Fig. 6 (A) The fluorescence intensity at 580 nm of CS-UCNP@mSiO$_2$-RBH (3 mg/mL) with Cu^{2+} (950 μM) as a function of time. (B) The fluorescence intensity at 580 nm of CS-UCNP@mSiO$_2$-RBH (3 mg/mL) in absolute ethanol solution of different pH in the absence (bottom line, square) and presence (top line, circle) of 950 μM Cu^{2+}. The pH of the solutions was adjusted by addition of 0.1 mol L^{-1} HCl (or 0.1 mol L^{-1} NaOH).

3.3 Luminescence imaging of intracellular Cu^{2+}

MTT assay was performed to assess the toxic nature of probe CS-UCNP@mSiO$_2$-RBH at the experimental concentration (Fig. S8). Assuming that the viability of untreated HeLa cells was 100%, the viabilities of HeLa cells still retained 90.0% after the incubation with probe for 24 h at 37 ^{o}C, even at a high concentration of 500 μg /mL, indicating that this Cu^{2+} fluorescent probe can be considered to be low cytotoxicity. These results demonstrate that CS-UCNP@mSiO$_2$-RBH can be used for monitoring Cu^{2+} within biological samples. Therefore, laser scanning confocal microscopy experiments were carried out to demonstrate the applicability of the CS-UCNP@mSiO$_2$-RBH in the bioimaging of intracellular Cu^{2+}. After incubating with 0.2 mg/mL of CS-UCNP@mSiO$_2$-RBH for 4 h at 37 ^{o}C and then supplemented with 10 μM CuCl$_2$ in the growth medium for 4 h at 37 ^{o}C, HeLa cells showed the green UCL emission at 520-560 nm under the excitation of 980 nm (Fig. 7b), and the emission at 560-600 nm was also observed obviously under the excitation of 543 nm with a HeNe laser (Fig. 7c). The overlay of brightfield (Fig. 7a) and fluorescence pictures indicated that

the nanoprobe could be used for monitoring subcellular distribution of Cu^{2+} in biological samples based on upconversion luminescence and downconversion fluorescence (Fig. 7d).
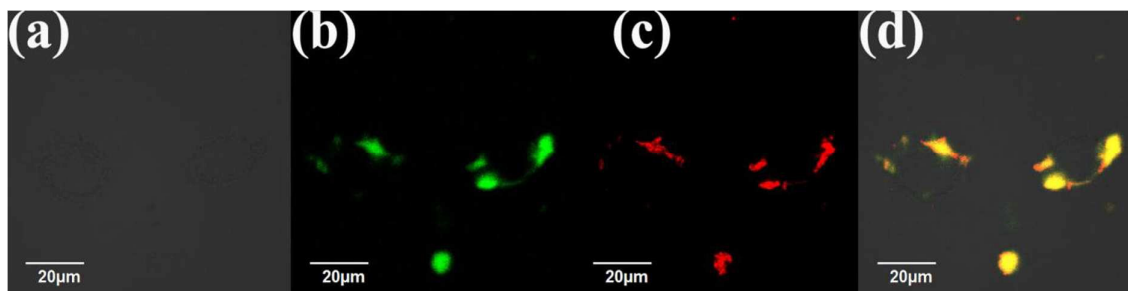

Fig. 7. Laser scanning confocal microscopy and bright field images of HeLa cells. (a) Bright field image, (b) upconversion luminescence image (λ_{ex}= 980 nm), (c) downconversion fluorescence image (λ_{ex}= 543 nm), and (d) overlay image of HeLa cells stained with 0.2 mg/mL CS-UCNP@mSiO$_2$-RBH for 4 h at 37 $^{\circ}$C and then incubated with 10 μM CuCl$_2$ in the growth medium for 4 h at 37 $^{\circ}$C.

4. Conclusion

In conclusion, we have reported a LRET nanoprobe in which core-shell structured lanthanide upconversion nanocrystals act as energy donor and a rhodamine B derivative (RBH) act as energy acceptor for the detection of Cu^{2+}. The nanoprobe caused an obvious color change for colorless to pink that can be seen by naked-eye and an enhancement of the fluorescence emission when upon the addition of Cu^{2+}. Upon 980 nm excitation, the intensity of green upconverting emission decreases gradually while a new emission appears at 580 nm enhanced with the increasing concentration of Cu^{2+}, corresponding to the efficient LRET from CS-UCNP to the RBH-Cu^{2+} complex. The obtained nanoprobe could detect Cu^{2+} exclusively even at the present of Hg^{2+} benefited by the one atom substituting in the rhodamine B derivative. Furthermore, laser scanning confocal microscopy experiments have established the utility of CS-UCNP@mSiO$_2$-RBH probe in monitoring Cu^{2+} within living cells, suggesting that this probe will be of great benefit to biomedical

researchers for studying the effects of Cu^{2+} in biological systems.

Reference

1.   C. M. Lim, M. A. Cater, J. F. Mercer and S. L. Fontaine, *Biochem. Biophys. Res. Commun.*, 2006, **348**, 428.

2.   K. J. Barnham, C. L. Masters and A. I. Bush, *Nat. Rev. Drug. Discov.*, 2004, **3**, 205.

3.   C. D. Syme, R. C. Nadal, S. E. Rigby and J. H. Viles, *J. Biol. Chem.*, 2004, **279**, 18169.

4.   G. Manfredi and Z. Xu, *Mitochondrion*, 2005, **5**, 77.

5.   J. Liu, C. Li and F. Li, *J. Mater. Chem.*, 2011, **21**, 7175.

6.   C. Li, J. Liu, S. Alonso, F. Li and Y. Zhang, *Nanoscale*, 2012, **4**, 60651.

7.   M. X. Yu, M. Shi, Z. G. Chen, F. Y. Li, X. X. Li, Y. H. Gao, J. Xu, H. Yang, Z. G. Zhou, T. Yi and C. H. Huang, *Chem. Eur. J.*, 2008, **14**, 6892.

8.   Z. H. Zhang, H. F. Ji, S. Zhang, D. L. Peng, Q. X. Fu, Mi. H. Wang, L. H. He and L. Y. Yue, *New J. Chem.*, 2016, **40**, 755.

9.   Y. Yuan, S. H. Sun, S. Liu, X. W. Song and X. J. Peng, *J. Mater. Chem. B*, 2015, **3**, 5261.

10.   G. Li, F. R. Tao, H. Wang, L. P. Wang, J. J. Zhang, P. P. Ge, L. Liu, Y. H. Tong and S. Sun. *RSC Adv.*, 2015, **5**, 18983.

11.   A. Rai, N. Kumari, R. Nair, K. Singh and L. Mishra. *RSC Adv.*, 2015, **5**, 14382.

12.   M. Li, X. J. Jiang, H. H. Wu, H. L. Lu, H. Y. Li, H. Xu, S. Q. Zang and T. C. W. Mak, *Dalton Trans.*, 2015, **44**, 17326.

13. X. Y. Guan, W. Y. Lin and W. M. Huang, *Org. Biomol. Chem.*, 2014, **12**, 3944.

14. Y. Fang, Y. Zhou, Q. Q. Rui and C. Yao, *Organometallics*, 2015, **34**, 2962.

15. M. Suresh, A. Shrivastav, S. Mishra, E. Suresh and A. Das, *Org. Lett.*, 2008, **10**, 3013.

16. X. Zeng, L. Dong, C. Wu, L. Mu, S. F. Xue and Z. Tao, *Sensor. Actuat. B-Chem.*, 2009, **141**, 506.

17. M. Suresh, S. Mishra, S. K. Mishra, E. Suresh, A. K. Mandal, A. Shrivastav and A. Das, *Org. Lett.*, 2009, **11**, 2741.

18. Q. Liu, Y. Sun, T. S. Yang, W. Feng, C. G. Li and F. Y. Li, *J. Am. Chem. Soc.*, 2011, **133**, 17122.

19. L. Z. Zhao, J. J. Peng, Q. Huang, C. Y. Li, M. Chen, Y. Sun, Q. N. Lin, L. Y. Zhu and F. Y. Li, *Adv. Funct. Mater.*, 2014, **24**, 363.

20. L. Q. Xiong, Z. G. Chen, M. X. Yu, F. Y. Li, C. Liu and C. H. Huang, *Biomaterials*, 2009, **30**, 5592.

21. J. Zhou, Z. Liu and F. Y. Li, *Chem. Soc. Rev.*, 2012, **41**, 1323.

22. S. Jeong, N. Won, J. Lee, J. Bang, J. Yoo, S. G. Kim, J. A. Chang, J. Kim and S. Kim, *Chem. Commun.*, 2011, **47**, 8022.

23. Z. Q. Guo, W. H. Zhu, M. M. Zhu, X. M. Wu and H. Tian, *Chemistry*, 2010, **16**, 14424.

24. S. A. Hilderbrand and R. Weissleder, *Curr. Opin. Chem. Biol.*, 2010, **14**, 71.

25. L. L. Li, R. B. Zhang, L. L. Yin, K. Z. Zheng, W. P. Qin, P. R. Selvin and Y. Lu, *Angew. Chem. Int. Ed.*, 2012, **51**, 6121.

26. Y. P. Du, B. Xu, T. Fu, M. Cai, F. Li, Y. Zhang and Q. B. Wang, *J. Am. Chem. Soc.*, 2010, **132**, 1470.

27. J. Zhou, Q. Liu, W. Feng, Y. Sun and F. Y. Li, *Chem. Rev.*, 2015, **115**, 395.

28.   Y. Cen, Y. M. Wu, X. J. Kong, S. Wu, R. Q. Yu and X. Chu, *Anal. Chem.*, 2014, **86**, 7119.

29.   S. J. Wu, N. Duan, Z. Shi, C. C. Fang and Z. P. Wang, *Talanta*, 2014, **128**, 327.

30.   C. H. Liu, Z. Wang, H. X. Jia and Z. P. Li, *Chem. Commun.*, 2011, **47**, 4661.

31.   Z. Q. Li and Y. Zhang, *Nanotechnology*, 2008, **19**, 345606.

32.   N. Lang and A. Tuel, *Chem. Mater.*, 2004, **16**, 1961.

33.   L. Q. Xiong, T. S. Yang, Y. Yang, C. J. Xu and F. Y. Li, *Biomaterials*, 2010, **31**, 7078.

34. A. D. Becke. *J. Chem. Phys.*, 1993, **98**, 5648.

35. C. Lee, W. Yang, and R. G. Parr, *Phys. Rev. B* 1988, **37**, 785.

36. A. D. Becke, *J. Chem. Phys.* 1993, **98**, 5648.

37. P. J. Hay, and W. R. Wadt, *J. Chem. Phys.* 1985, **82**, 270.

38. W. R. Wadt, and P. J. Hay, *J. Chem. Phys.* 1985, **82**, 284.

39. P. J. Hay, and W. R. Wadt, *J. Chem. Phys.* 1985, **82**, 299.

40. M. M. Francl, W. J. Pietro, W. J. Hehre, J. S. Binkley, M. S. Gordon, D. J. DeFrees, and J. A. Pople, *J. Chem. Phys.*, 1982, **77**, 3654.

41. V. Barone, and M. Cossi, *J. Phys. Chem. A* 1998, **102**, 1995–2001.

42. M. J. Frisch, G. W. Trucks, H. B. Schlegel, G. E. Scuseria, M. A. Robb, J. R. Cheeseman, G. Scalmani, V. Barone, B. Mennucci, G. A. Petersson, H. Nakatsuji, M. Caricato, X. Li, H. P. Hratchian, A. F. Izmaylov, J. Bloino, G. Zheng, J. L. Sonnenberg, M. Hada, M. Ehara, K. Toyota, R. Fukuda, J. Hasegawa, M. Ishida, T. Nakajima, Y. Honda, O. Kitao, H. Nakai, T. Vreven, J. A. Montgomery, J. E. Peralta, F. Ogliaro, M. Bearpark, J. J. Heyd, E. Brothers, K. N. Kudin, V. N. Staroverov, R. Kobayashi, J. Normand, K. Raghavachari, A. Rendell, J. C. Burant, S. S. Iyengar, J. Tomasi, M. Cossi, N. Rega, J. M. Millam, M. Klene, J. E. Knox, J. B. Cross, V. Bakken, C. Adamo, J. Jaramillo, R. Gomperts, R. E. Stratmann, O. Yazyev, A. J. Austin, R.

Cammi, C. Pomelli, J. W. Ochterski, R. L. Martin, K. Morokuma, V. G. Zakrzewski, G. A. Voth, P. Salvador, J. J. Dannenberg, S. Dapprich, A. D. Daniels, Farkas, J. B. Foresman, J. V. Ortiz, J. Cioslowski, and D. J. Fox, *Gaussian 09, Revision D.01;* Gaussian Inc., 2009, Wallingford, CT.

43. Q. Liu, M. Chen, Y. Sun, G.Y. Chen, T. S. Yang, Y. Gao, X. Z. Zhang and F. Y. Li, *Biomaterials*, 2011, **32**, 8243.

<div align="center">

TOC Graphic

</div>

A new organic-inorganic hybrid nanoprobe based on luminescence resonance energy transfer (LRET) from mesoporous silica coated upconversion nanoparticles to rhodamine B derivative was prepared for distinguish Cu^{2+} from Hg^{2+} and living cells imaging application.